Electronic Supplementary Material (ESI) for Catalysis Science & Technology.

Supporting Information

Facile synthesis of impurity-free iron single-atom catalysts for highly efficient oxygen reduction reaction

Qian He,‡[a] Yuying Meng,‡[ab] Hao Zhang,[a] Ying Zhang,[a] Hongyu Chen,[a] Xiaohui He,*[a] Mingmei Wu,*[a] and Hongbing Ji*[ac]

[a] *Fine Chemical Industry Research Institute, School of Chemistry, Sun Yat-sen University, No. 135, Xingang Xi Road, Guangzhou 510275, P. R. China*

[b] *Institute of Advanced Wear & Corrosion Resistant and Functional Materials, Jinan University, No. 601, Huangpu Road, Guangzhou 510632, P. R. China*

[c] *School of Chemical Engineering, Guangdong University of Petrochemical Technology, No. 139, Guandu Two Road, Maoming 525000, P.R.China*

*Corresponding authors： jihb@mail.sysu.edu.cn (Prof. H. Ji)
ceswmm@mail.sysu.edu.cn (Prof. M. Wu)
hexiaohui@mail.sysu.edu.cn (Dr. X. He)

‡ Co-first authors: these authors contributed equally to this work.

Table of Contents

1. Experimental Section

Chemical and Reagents

Pyrrole (99%), *N,N*-dimethylformamide (DMF, 99.9%), tetrahydrofuran (99.9%), triethylamine (99.9%), isopropyl alcohol (99.9%), dichloromethane (99.9%), hexane (99.5%), and methanol (MeOH, 99.9%), 2,2'-azobisisobutyronitrile (AIBN, 99%), iron oxide (Fe_2O_3, 99.9%) were purchased from Aladdin. Propionic acid (99.9%), iron(II) chloride ($FeCl_2$, 99.9%) were obtained from J＆K. 4-vinylbenzaldehyde were purchased from Huaweiruike Chemical. Tetraphenylporphyrin iron(III) chloride (FeTPPCl, 98%) and silica gel (200–300 mesh) were bought from Yuanjiang Hualong and Qingdao Haiyang Chemical Plant, respectively. Platinum on activated carbon (20 wt% Pt/C) and Nafion solution (5 wt%) were bought from Johnson Matthey and DoPont company, respectively. Pyrrole was distilled under a N_2 atmosphere before each time using. Other chemical reagents were employed as received without further purification.

Synthesis

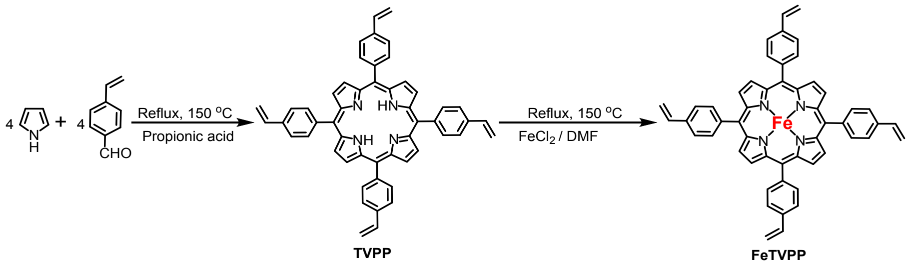

Figure S1. Schematic illustration for synthesis of TVPP and FeTVPP.

Synthesis of tetra(4'-vinylphenyl)porphyrin (TVPP): The TVPP was synthesized by a "one-pot" reaction. Typically, 13.2 g 4-vinylbenzaldehyde (100 mmol) was added to a two-necked round-bottomed flask (1000 mL) containing 500 mL propionic acid, and then the mixture was heated to 140 °C, followed by addition of 6.7 g freshly distilled pyrrole (100 mmol). After refluxing for 3 h at 140 °C, the solution was cooled to room temperature naturally. Subsequently, the as-obtained precipitate was filtered, washed with methanol and dried in the air. The precipitate was further purified with silica gel column chromatography using CH_2Cl_2 as eluent. After removal of eluent by rotary evaporation, the product was dried at 80 °C in vacuum for 24 h and gave the purple powder with the yield of 15%. ^1H NMR (500 MHz, $CDCl_3$): δ 8.89 (s, 8H, β-porph-H), 8.18–8.19 (d, 8H, J = 8.2 Hz, Ph-H), 7.80–7.81 (d, 8H, J = 7.8 Hz, Ph-H), 7.04–7.10 (m, 4H, CH=), 6.06–6.09 (d, 4H, J = 6.1 Hz, $=CH_2$), 5.49–5.51 (d,4H, J = 5.5 Hz, $=CH_2$), and -2.78 (s, 2H, N–H) ppm. MALDI-TOF MS: m/z calcd, 718.90; found, 718.30.

Synthesis of tetra(4'-vinylphenyl)porphyrin iron (FeTVPP): 0.72 g the as-synthesized TVPP (1.0 mmol) and 0.63 g iron(II) chloride ($FeCl_2$, 5.0 mmol) were dissolved in 150 mL *N,N*-dimethylformamide (DMF) in a 250 mL three-necked round-bottomed flask under the N_2 atmosphere. After refluxing for 3 h at 150 °C, the solution was cooled to room temperature naturally. After removal of DMF solvent by rotary evaporation, the material was purified by silica gel column chromatography with CH_2Cl_2/MeOH (10/1, v/v) as eluent, producing brown powder (named as FeTVPP) with the yield of 83%. MALDI-TOF MS ($[M-Cl]^+$): m/z calcd, 772.73; found, 772.20.

Synthesis of poly-FeTVPP: 58.9 mg FeTVPP (0.075 mmol), 1.08 g TVPP (1.5 mmol) (FeTVPP:TVPP = 1:20 mmol:mmol), and 98.5 mg AIBN(0.6 mmol) were added in a three-necked round-bottomed flask (125 mL) containing 50 mL DMF under the N_2 atmosphere, followed by refluxing at 180 °C for 24 h. After cooling down to room temperature, the solution was filtered and washed with MeOH, THF, and DMF, respectively, giving the fluffy crude product. Then, the material was further purified by Soxhlet extractions for 24 h using methanol and dichloromethane, respectively. After drying in vacuum oven for 24 h at 80 °C, the black material was obtained.

Synthesis of Fe-N-C-T: The above resulting material poly-FeTVPP was placed in a temperature-programmable tube furnace and subjected to the following thermal treatments in a flow of N_2 at a rate of 100 mL/min. The furnace temperature was firstly increased from room temperature (i.e. 25 °C) to a final pyrolysis temperature (i.e.900 °C) at a heating rate of 5 °C min^{-1}, and kept at this temperature for 3 h. The furnace was then let to cool down to room temperature, after which a black-colored powder product was obtained. By tuning the final heat treatment temperature (700, 800, 900, 1000, 1100 °C), different Fe-based materials named as Fe-N-C-T, were obtained, where T represents the final heat treatment temperature.

Synthesis of poly-TVPP: Similarly, poly-TVPP was also synthesized with the same procedure of poly-FeTVPP and used FeTVPP:TVPP = 0:1 mmol:mmol instead.

Synthesis of N-C-900: Similar as Fe-N-C-T, the N-C-900 was obtained by pyrolysis poly-TVPP at 900 °C.

Synthesis of Fe-NPs/N-C-900: 5 ml $FeCl_2$ solutions (10 mmol/L, H_2O:MeOH = 1:1, V:V) was added to 1g poly-TVPP and stirred for 30 min at room temperature. After removal of solvents by rotary evaporation, the material was treated as Fe-N-C-900 (pyrolysis at 900 °C) to obtain Fe-NPs/N-C-900.

All the synthesized materials were complied in Table S1.

Table S1. Samples obtained from different synthetic conditions.

Catalyst	MTVPP:TVPP (mmol:mmol)	Pyrolysis temperature (°C)
Poly-FeTVPP	1:20	—
Fe-N-C-700	1:20	700
Fe-N-C-800	1:20	800
Fe-N-C-900	1:20	900
Fe-N-C-1000	1:20	1000
Fe-N-C-1100	1:20	1100
Poly-TVPP	0:1	—
N-C-900	0:1	900
Fe-NPs/N-C-900[a]	0:1	900

[a] Added with $FeCl_2$ solutions (5 ml, 10 mmol/L, H_2O:MeOH = 1:1, V:V)

Characterization.

The crystal structure of the as-synthesized materials was investigated by powder X-ray diffraction (XRD) on Bruker D8 Advanced diffractometer operating with Cu Kα radiation (λ =1.5418 Å). The XRD patterns were obtained in a 2θ range from 10 ° to 80 ° at a scan rate of 5 ° min^{-1}. Elemental analysis (EA) was performed on Vario EL cube instrument. Inductively coupled plasma optical emission spectroscopy (ICP-OES) was obtained by PerkinElmer OPTIMA 8000DV. X-ray photoelectron spectroscopy (XPS) analysis was carried out to determine the element composition on an ESCALAB 250 X-ray photoelectron system operating with a monochromatic X-ray source (Al Kα hv = 1486.6 eV), where the C 1s peak position of 284.8 eV was used to calibrate the energy scale. The standard deviations of the survey scans and high-resolution scans of the individual peaks were 1 and 0.1 eV. A Renishaw Raman system model in Via spectrometer operating with a 20 mW air-cooled argon ion laser (λ = 514.5 nm) as the excitation source was used to study the Raman spectra. The nitrogen adsorption and desorption isotherms of the materials were obtained with a N_2 Micromeritic ASAP2020M at the liquid-N_2 temperature. In order to remove any possible guest species adsorbed on the samples' surfaces before each measurement, the samples were degassed in vacuum at 300 °C for 6 h. From the adsorption/desorption data, the Brunauer-Emmett-Teller (BET) surface areas of the materials were then determined. Transmission electron microscopy (TEM) images and scanning transmission electron microscopy (STEM) images were obtained on FEI Tecnai G2 F30 equipped with high-angle annular dark field (HAADF) with an accelerating voltage of 300 kV. Aberration corrected high-angle annular dark-field scanning transmission electron microscopy (AC HAADF-STEM) images and energy dispersive X-ray spectroscopy (EDS) mapping images were obtained on a JEM-ARM200F transmission electron microscopy operated at 200 kV, which incorporated with double spherical aberration correctors and a super-X EDS system. The extended X-ray absorption fine structure spectra (EXAFS) and the X-ray absorption near-edge structure (EANES) of Fe k^3-edge were performed in fluorescence mode on BL14W1 beamline at the Shanghai Synchrotron Radiation Facility, Shanghai Institute of Applied Physics, China, operated at 3.5 GeV with injection currents of 140–210 mA and monochromatized with Si(111) double-crystal. Fe foil, Fe_2O_3, and FeTPPCl were used as reference samples.

Electrocatalytic Performance Test.

The electrocatalytic performances toward oxygen reduction reaction (ORR) of all the catalysts were performed on a Pine Bipotentiostat (Pine Research Instrumentation) and a three-electrode system in 0.1 M KOH at room temperature was taken, where a rotating disk electrode (RDE, diameter: 5.0 mm) coated with catalysts was used as the working electrode, graphitic carbon rod (diameter: 3,0 mm) and saturated Ag/AgCl were employed as the counter and reference electrodes, respectively. All potentials were conversed to the reversible hydrogen electrode (RHE) by Nernst equation, Eq. S1:

$$E\ (\mathrm{V}\ vs.\ \mathrm{RHE}) = E\ (\mathrm{V}\ vs.\ \mathrm{Ag/AgCl}) + 0.197 + 0.059\ \mathrm{pH}. \qquad \text{Eq. S1}$$

To prepare the working electrode, the following procedures were used: 1) 2.00 mg of the electrocatalyst was mixed with 400 μL of isopropanol and then sonicated at least 30 min, forming a homogeneous ink suspension; 2) 4 μL of the electrocatalyst suspension was dropped onto the surface of a freshly polished RDE with the loading of 0.255 mg cm^{-2} and allowed to dry under air; 3) 2.0 μL of 0.5 wt% Nafion solution was cast onto the electrode and allowed to completely dry under ambient conditions to protect the electrocatalyst film. After 30 cycles activation in either O_{2}- or N_2-saturated 0.1 M KOH solution, CVs for different electrocatalysts were recorded from 1.07 to 0.17 V (*vs.* RHE) with a scan rate of 100 mV s^{-1}. Then, the LSVs were obtained at a sweep rate of 10 mV s^{-1} in O_2-saturated 0.1 M KOH solution with variable rotating speed (400, 625, 900, 1225, 1600, 2025, 2500 rmp).

The electrons transfer number (*n*) per oxygen molecule involved in ORR was evaluated by two methods. The first one is using Koutecky-Levich (K-L) equation,[1] Eq. S2–4:

$$\frac{1}{J} = \frac{1}{J_\mathrm{K}} + \frac{1}{J_\mathrm{L}} = \frac{1}{J_\mathrm{K}} + \frac{1}{B\omega^{1/2}} \qquad \text{Eq. S2}$$

$$B = 0.62nFC_0(D_0)^{2/3}\upsilon^{-1/6}$$

Eq. S3

$$J_K = nFkC_0$$

Eq. S4

where, J is the measured current density, J_L and J_K are the diffusion- and kinetic-limiting current densities, ω is the angular speed of the rotating electrode, n is the involved electron transfer number, F is the Faraday constant, k is the electro-transfer rate constant for oxygen reduction, C_0 is the saturated O_2 concentration in the electrolyte, D_0 is the diffusion coefficient of O_2 in the electrolyte, and v is the kinetic viscosity of the solution. In our work, $F = 9.65 \times 104$ C mol^{-1}, $C_0 = 1.2 \times 10^{-6}$ mol cm^{-3}, $D_0 = 1.9 \times 10^{-5}$ cm^2 s^{-1} and $v = 0.01$ cm^2 s^{-1} were used. The values of n and J_K were obtained from the slope and y-intercept of the *K-L* plots (or $1/J$ *vs.* $\omega^{-1/2}$), respectively.

In addition, n along with the yield of hydrogen peroxide (H_2O_2) relative to the total products were also determined by the rotating ring-disk electrode (RRDE) technique at a speed of 1600 rpm.[2] Eq. S5–6:

$$n = \frac{4J_D}{J_D + \frac{J_R}{N}}$$

Eq. S5

$$H_2O_2\% = 200 \times \frac{\frac{J_R}{N}}{J_D + \frac{J_R}{N}}$$

Eq. S6

Where, J_D and J_R are the disk and ring current densities in the RRDE, and N is the collection efficiency of the Pt ring electrode. In our case, the potential of Pt ring electrode was set as 1.317 V (*vs.* RHE) and N was found to be 0.37.

2. Supplementary Figures and Tables

Table S2. Physical properties, compositional information, and BET surface area for the synthesized catalysts

Catalyst	M (wt%)[a]	N (wt%)[b]	BET surface area (m^2g^{-1}) [c]
Fe-N-C-700	0.43	4.87	808
Fe-N-C-800	0.45	3.64	1048
Fe-N-C-900	0.47	2.39	1490
Fe-N-C-1000	0.52	1.72	1105
Fe-N-C-1100	0.55	1.42	925
N-C-900	—	2.35	1350
Fe-NPs/N-C-900	0.63	2.41	1233

[a] obtained from ICP-OES. [b] obtained from EA. [c] Sorption isotherm of N_2 at 77 K.

Table S3. Metal content of Fe-N-C-900

Metal	Content (wt%)[a]
Fe	0.47
Na	0.0002
M[b]	<0.0001

[a] obtained from ICP-OES. [b] M = Mg, Ca, Ti, V, Cr, Mn, Co, Ni, Cu, Zn, Y, Zr, Nb, Mo, Ru, Rh, Pd, Ag, Cd, Sn, W, Ir, Pt, and Au)

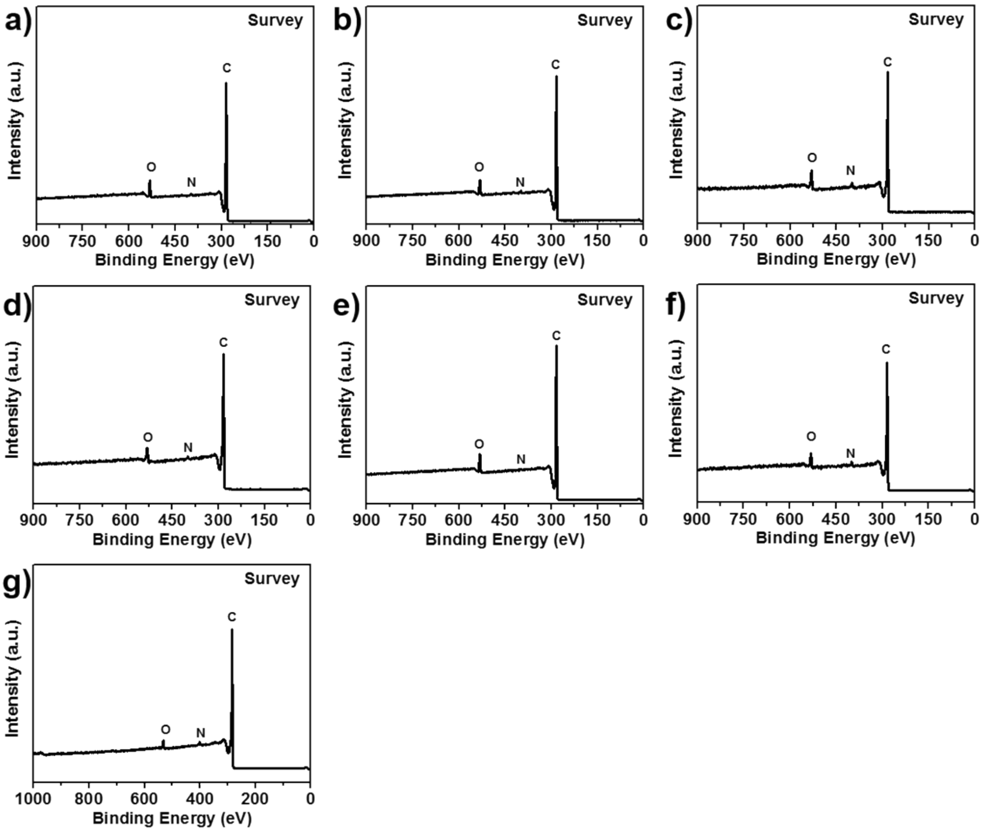

Figure S2. Survey XPS spectrum of Fe-N-C-T (a, T = 700; b, T = 800; c, T = 900; d, T = 1000; e, T = 1100; respectively), N-C-900 (f), and Fe-NPs/N-C-900 (g).

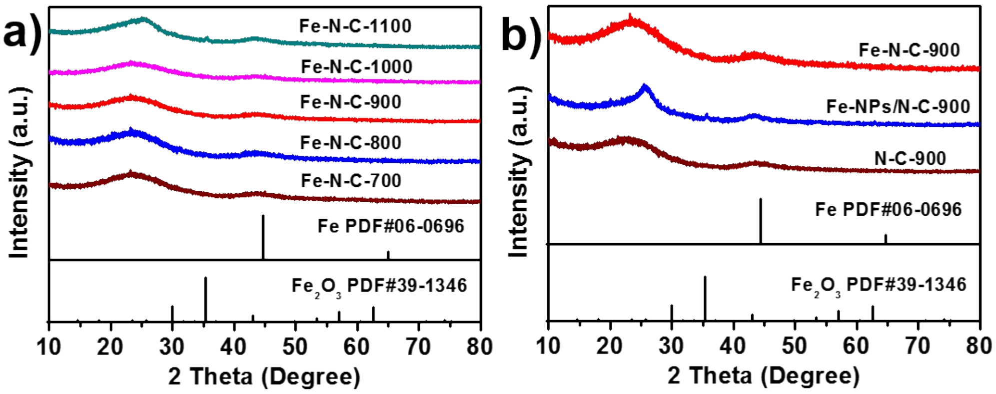

Figure S3. XRD patterns of a) Fe-N-C-T materials (T = 700, 800, 900 or 1000, 1100 °C) and b) Fe-N-C-900, Fe-NPs/N-C-900, and N-C-900.

Table S4. Parameter of EXAFS fitting for the Fe-N-C-900

Sample	Shell	Coordination number	Bond length R (Å)	Bond disorder σ^2 ($\times$ 10^{-3}Å^2) [a]	ΔE/eV [b]
Fe-N-C-900	Fe–N(O)	5.8±0.5	2.01±0.01	7	2.3

[a] Debye-waller factors; [b]: the inner potential correction.

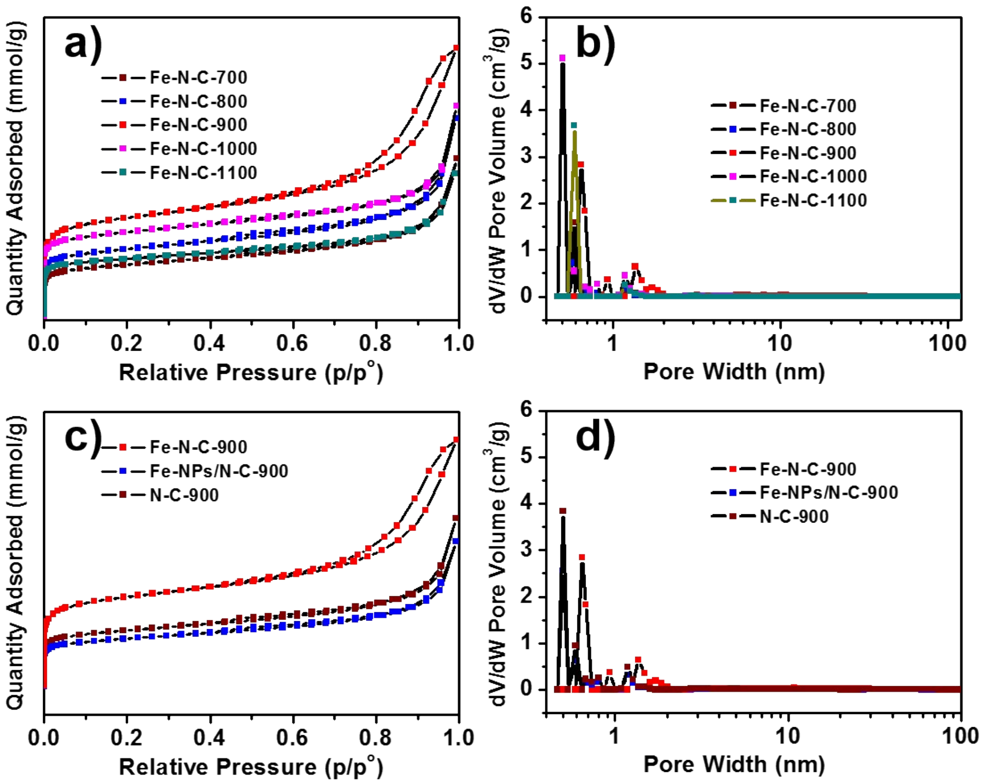

Figure S4. a) N_2 adsorption/desorption isotherms and b) BJH pore size distributions of Fe-N-C-T materials (T = 700, 800, 900, 1000 or 1000 °C). c) N_2 adsorption/desorption isotherms and b) BJH pore size distributions of Fe-N-C-900, Fe-NPs/N-C-900, and N-C-900.

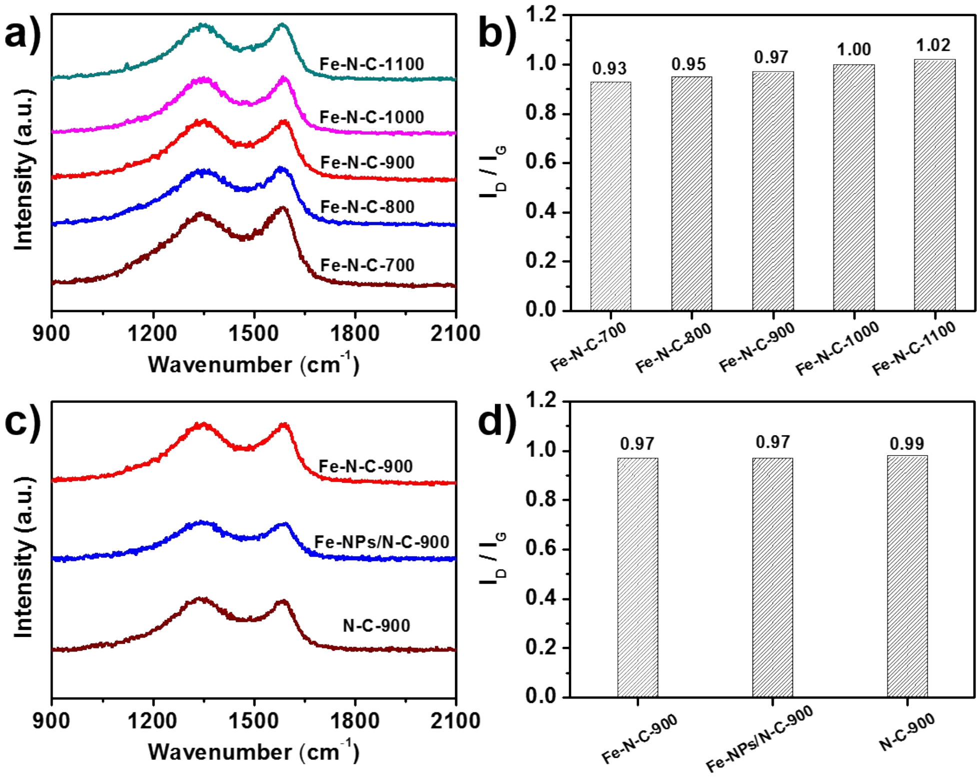

Figure S5. a) Raman spectra and b) I_D/I_G ratios of Fe-N-C-T materials (T = 700, 800, 900, 1000 or 1100 °C). c) Raman spectra and d) I_D/I_G ratios of Fe-N-C-900, Fe-NPs/N-C-900, and N-C-900.

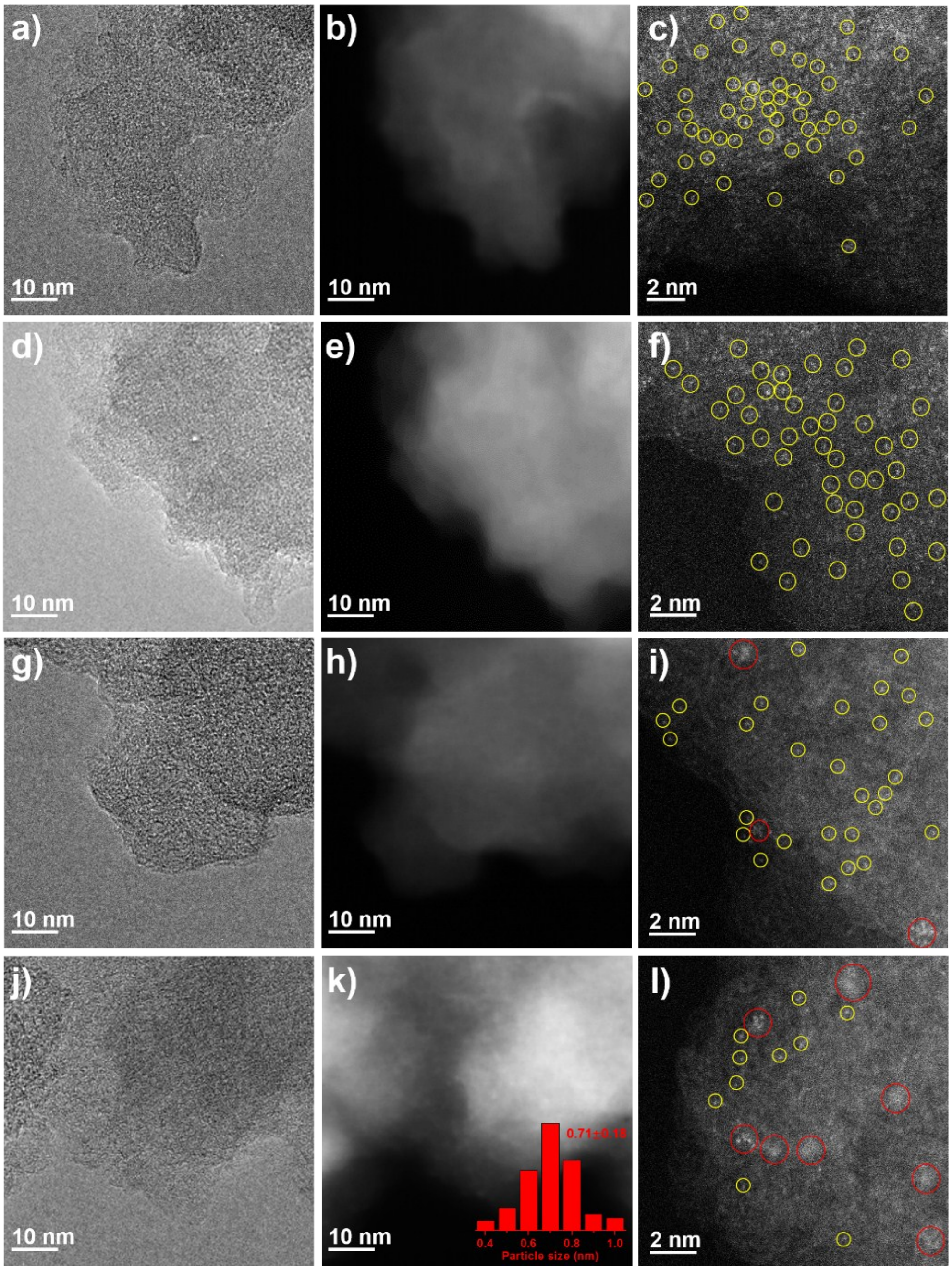

Figure S6. TEM image (left), STEM image (middle), and AC HAADF-STEM image (right) of Fe-N-C-T (a–c, T = 700; d–f, T = 800; g–i, T = 1000; j–l, T = 1100), respectively. Fe single atoms were highlighted by yellow circles, Fe nanoclusters were highlighted by red circles.

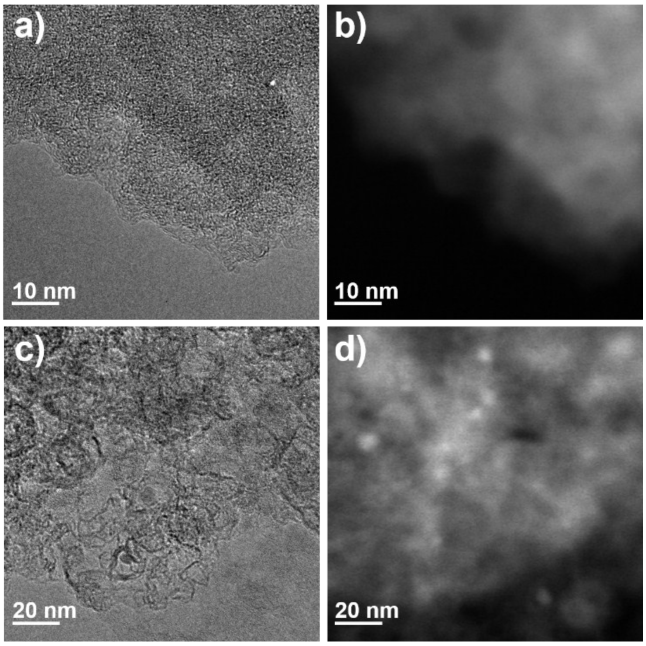

Figure S7. TEM image (left) and STEM image (right) of N-C-900 (a–b) and Fe-NPs/N-C-900 (c–d), respectively.

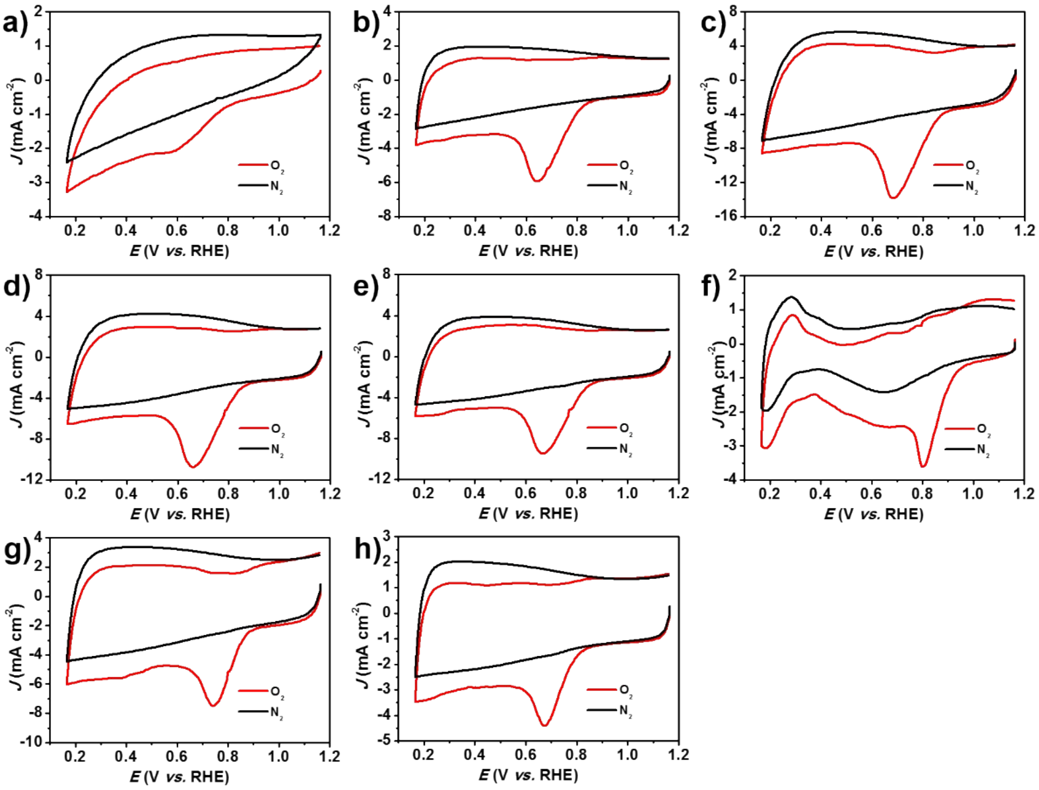

Figure S8. CV curves of catalysts in O$_2$-saturated 0.1 M KOH solution. a–e) for Fe-N-C-T (T = 700, 800, 900, 1000 or 1100 °C), f) for 20 wt% Pt/C, g) for Fe-NPs/N-C-900, and h) for N-C-900, respectively.

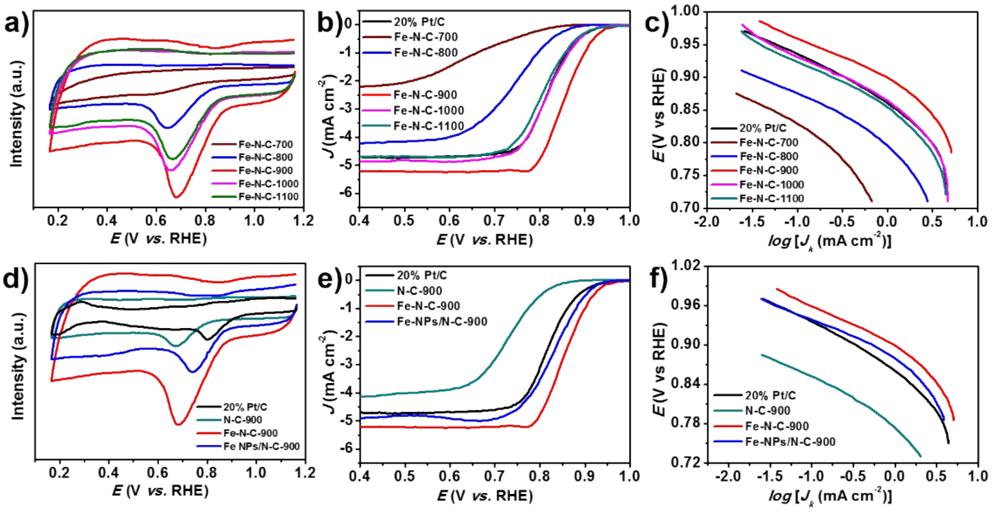

Figure S9. a) CV curves of Fe-N-C-T in O_2-saturated 0.1 M KOH solution. b) Kinetic current density (J_k) and c) Tafel curves of different Fe-N-C-T (T = 700, 800, 900, 1000 or 1100 °C) and 20 wt% Pt/C catalyst materials at 1600 rpm. d) CV curves in O_2-saturated 0.1 M KOH solution, e) Kinetic current density (J_k) and f) Tafel curves of 20 wt% Pt/C, N-C-900, Fe-N-C-900, and Fe-NPs/N-C-900 catalysts materials at 1600 rpm.

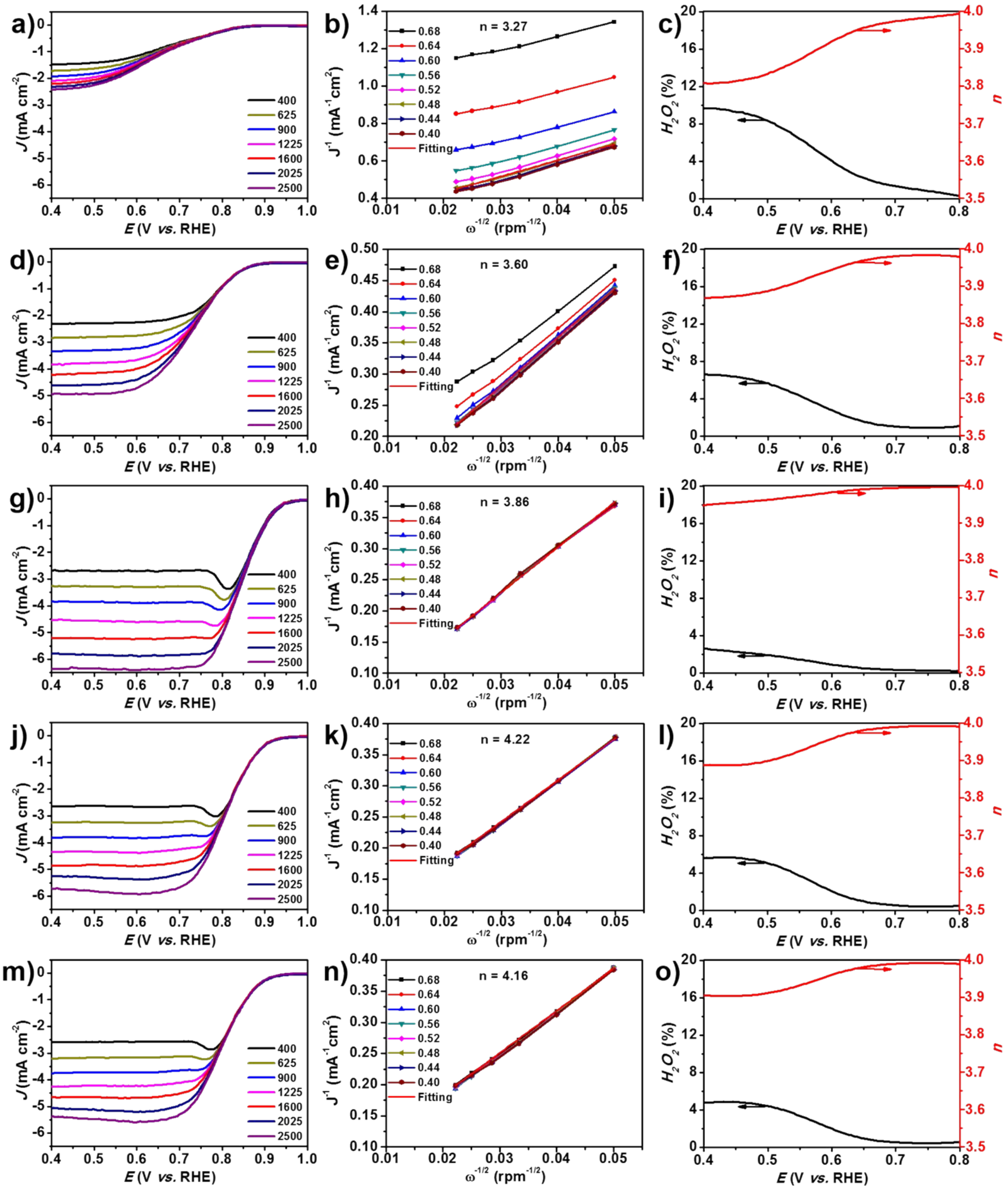

Figure S10. Polarization curves of ORR over catalysts on RDE rotating at different rotation speeds (left), K-L plots of catalysts at various potentials of ORR (middle), and the H_2O_2 yield and electron transfer number (n) of catalysts in ORR used RRDE as working electrode at 1600 rpm (right). Fe-N-C-T (a–c, T = 700; d–f, T = 800; g–i, T = 900; j–l, T = 1000; m–o, T = 1100; respectively).

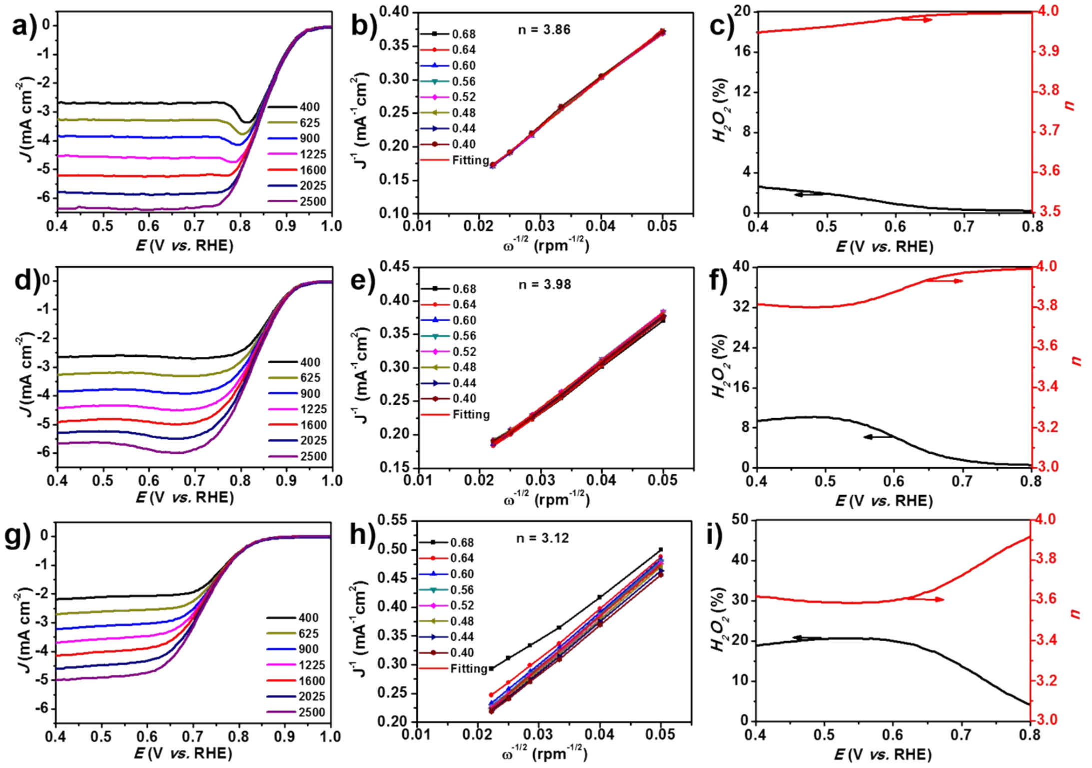

Figure S11. Polarization curves of ORR over catalysts on RDE rotating at different rotation speeds (left), K-L plots of catalysts at various potentials of ORR (middle), and the H_2O_2 yield and electron transfer number (n) of catalysts in ORR used RRDE as working electrode at 1600 rpm (right). Fe-N-C-900 (a–c), Fe-NPs/N-C-900 (d–f), and N-C-900 (g–i), respectively.

Table S5. E_{onset}, $E_{1/2}$, and J_K for corresponding catalysts in 0.1 M KOH solution[a]

Samples	E_{onset} (V *vs.* RHE)	$E_{1/2}$ (V *vs.* RHE)	J_K (mA cm^{-2})
Fe-N-C-700	0.85	0.65	2.22
Fe-N-C-800	0.87	0.74	4.22
Fe-N-C-900	0.96	0.86	5.21
Fe-N-C-1000	0.93	0.82	4.88
Fe-N-C-1100	0.93	0.81	4.66
N-C-900	0.85	0.73	4.15
Fe-NPs/N-C-900	0.94	0.84	4.92
20% Pt/C	0.93	0.82	4.71

[a] Three-electrode system at room temperature, used Ag/AgCl (saturated KCl solution), graphite rod and glass carbon rotating disk electrode (RDE, 5.00 mm) as reference, counter electrode and working electrode, respectively.

Table S6. Comparison of ORR performances in 0.1 M KOH of different single atoms materials.

Samples	E_{onset} (V *vs.* RHE)	$E_{1/2}$ (V *vs.* RHE)	J_K (mA cm^{-2})	References
Fe-N-C-900	0.96	0.86	5.21	This work
FeBNC-800	0.968	0.838	5.51	*ACS Energy Lett.*, 2018, **3**, 252–260
FeNx-PNC	0.997	0.86	5.95	*ACS Nano*, 2018, **12**, 1949–1958
FePc-RCNTs	0.951	0.860	5.62	*J. Power Sources*, 2018, **389**, 260–266
FePcZnPor-CMP	0.936	0.866	5.59	*J. Mater. Chem. A*, 2018, **6**, 22851–22857
Co@MCM	0.95	0.78	4.8	*Energy. Environ. Sci.*, 2018, **11**, 1980–1984
Co@C-N-120-900	0.956	0.851	5.6	*Inorg. Chem. Front.*, 2017, **4**, 1748–1756
Co SAs/N-C	0.982	0.881	5.5	*Angew. Chem. Int. Ed.*, 2016, **55**, 10800–10805

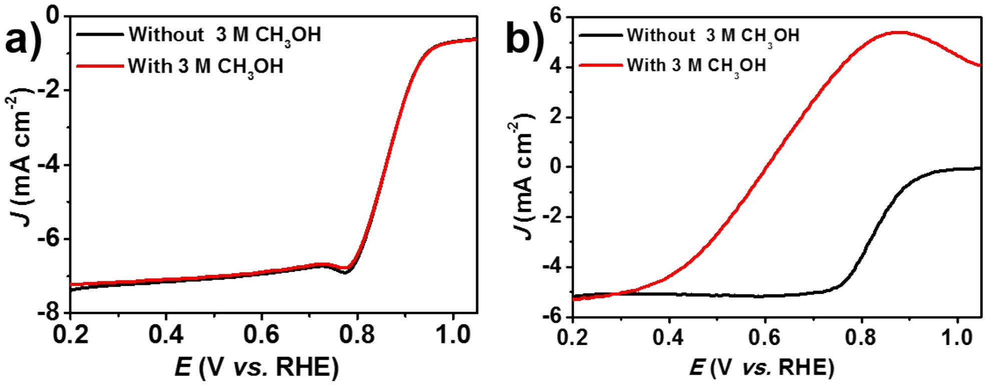

Figure S12. Tolerance test of a) Fe-N-C-900 and b) 20 wt% Pt/C in O_2-saturated 0.1 M KOH solution with and without of 3 M methanol.

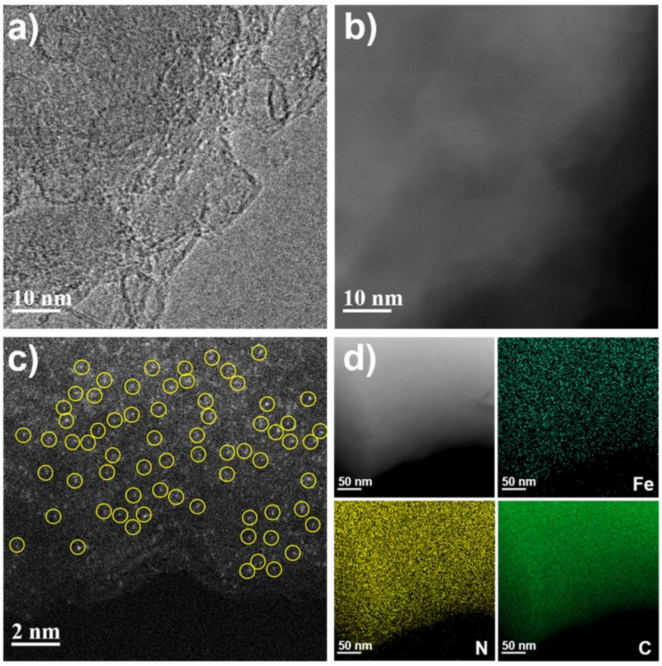

Figure S13. a) TEM image, b) STEM image, c) AC HAADF-STEM image (Fe single atoms were highlighted by yellow circles), and d) elemental mapping of Fe-N-C-900-used.

3. References

1 M. S. El-Deab and T. Ohsaka, *Electrochim. Acta*, 2002, **47**, 4255–4261.

2 Y. Liang, Y. Li, H. Wang, J. Zhou, J. Wang, T. Regier and H. Dai, *Nat. Mater.*, 2011, **10**, 780–786.